7A.1 National Mosaic and QPE (NMQ) System – Description, Results and Future Plans

NOAA/OAR/NSSL: Jian Zhang, Kenneth Howard, Steve Vasiloff, Carrie Langston, Brian Kaney, Ami Arthur, Suzanne Van Cooten, and Kevin Kelleher
NOAA/NWS/OHD: David Kitzmiller, Feng Ding, and Dong-Jun Seo
NOAA/NWS/OCWWS: Mary Mullusky, Ernie Wells
NOAA/OAR/ESRL/PSD: Tim Schneider
Salt River Project: Chuck Dempsey

1. Introduction

The National Mosaic and Multi-sensor QPE (Quantitative Precipitation Estimation), or "NMQ", system was initially developed from a joint initiative between the National Oceanic and Atmospheric Administration/National Severe Storms Laboratory, Salt River Project (SRP) and the Federal Aviation Administration/Aviation Weather Research Program. Further development has continued with additional support from the National Weather Service (NWS) Office of Hydrological Development and the NWS Office of Climate, Water, and Weather Services. The objective of NMQ research and development is twofold. The first is to develop a hydrometeorological platform for assimilating different observational networks and for creating high spatial and temporal resolution multi-sensor QPEs for flood warnings and water resource management on the national scale. The platform facilitates systematic evaluations and advances of hydrometeorological sciences. The second is to develop, for operational prototyping and utilization, a seamless high-resolution national 3-D grid of radar reflectivity for data assimilation, numerical weather prediction model verification, and aviation product development.

Through 10 years (1998-2007) of research and development, a real-time NMQ system has been implemented (http://nmq.ou.edu). Since June 2006, the system has been generating high-resolution 3-D reflectivity mosaic grids (31 vertical levels) and a suite of severe weather and QPE products for Conterminous United States at a 1-km horizontal resolution and 5 minute update cycle. The experimental products are provided to users from government agencies and universities in real-time and have been utilized in various meteorological, aviation, and hydrological applications. This paper describes various scientific components in the NMQ system and presents initial evaluation results and future plans of the system.

2. System Overview

An overview flowchart of the NMQ system is shown in Fig.1. Multiple data sources are used in four major modules that comprise the NMQ system: 1) single radar processing; 2) 3-D and 2-D radar mosaic; 3) Q2 (the next generation QPE, Vasiloff et al. 2007); and 4) evaluation. The data sources include the level-2 (base level) data from the NEXRAD network, RUC (Rapid Update Cycle, Benjamin et al. 2004) model hourly analyses, and rain gauge observations from the HADS (Hydrometeorological Automated Data System, http://www.nws.noaa.gov/oh/hads/WhatIsHADS.html) network. Descriptions of each module are provided below.

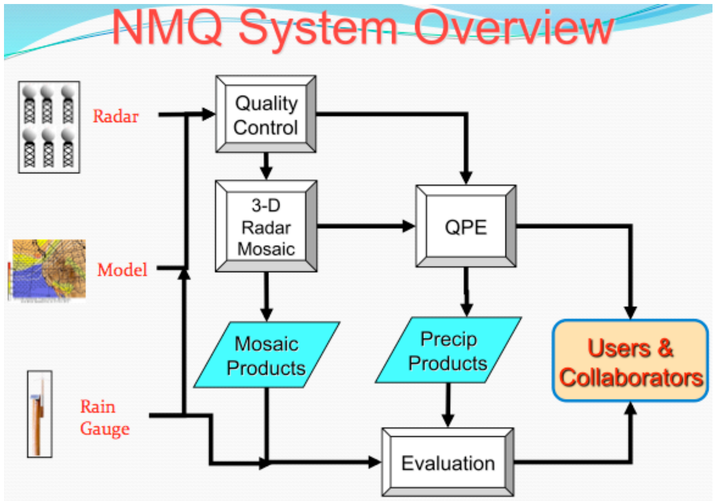

Fig. 1 An overview flowchart of the NMQ system.

2.1 Single radar processes

There are four scientific algorithms in the single radar processing: 1) reflectivity quality control (QC), 2) single radar Cartesian (SRC) grid, 3) vertical profile of reflectivity (VPR), and 4) single radar hybrid scan reflectivity.

The base level radar reflectivity data are QC'ed to remove non-precipitation echoes, including those from clear air, biological targets (birds and insects), residual ground clutter, electronic interference, and anomalous propagations. The reflectivity QC module includes a pre-processing, a neural network, and a post-processing. The neural network approach is based on 3-D spatial characteristics of reflectivity (Lakshmanan et al. 2007) such as intensity, gradients, texture, and depth of radar echoes. All the reflectivity bins with significant blockages or too close to the terrain (i.e., if the bottom of the bin is within 50 meters of the ground) are removed in the pre-processing. The pre- and post-processing utilize spatial and temporal image filters and heuristic rules (e.g., Zhang et al. 2004) based on radar scan mode and environmental data to remove specific non-precipitation echoes such as speckles, sun strobes (Figs.2a and 2b), clear air and biological returns. For instance, the total area of radar echoes in two consecutive volume scans is compared and if the increase in the area exceeds a certain threshold, the volume scan is considered to contain a hardware testing signal (i.e., echoes around KMBX radar, Figs.2c and 2d) and the data are discarded. Another example of the heuristic rules is for removing the so-called "bloom" echoes that are returns from migrating insects and birds and anomalous propagation (AP) due to nocturnal radiation cooling near the surface. When a radar is running in clear air modes and the surface temperature at the radar site is above 5°C, all the echoes in the volume scan are removed (Figs.2e and 2f).

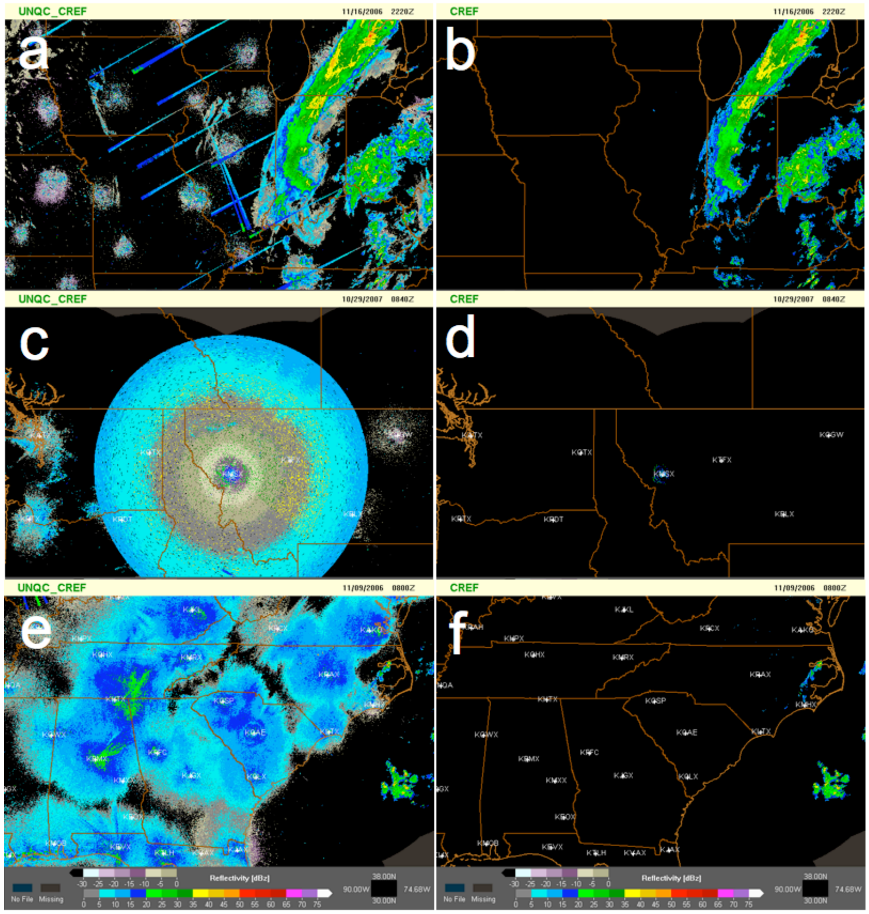

Fig. 2 Composite reflectivities before (a, c, e) and after (b, d, f) quality control. The composite reflectivities are valid at 22:20UTC on Nov. 16, 2006 (a, b), 08:40UTC on Oct. 29, 2007 (c and d), and 08:00UTC on Nov. 9, 2006 (e and f).

Each volume scan of QC'ed reflectivity field is interpolated from the spherical coordinate system onto a 3-D Cartesian grid that is centered on the radar's location. The Cartesian grid covers 460 km range for coastal radars and 300 km for inland radars. It has a horizontal resolution of 0.01° latitude/longitude (~1 km x 1 km), and 31 levels ranging from 500 m to 18 km above mean sea level. The analysis scheme includes a nearest neighbor approach on the range-azimuth plane and an exponential interpolation in the elevation direction (Zhang et al. 2005; Lakshmanan et al. 2006). The vertical influence of radar observations is confined between half a beam width above the highest elevation angle at the top and half a beam width below the lowest elevation angle at the bottom.

Vertical profiles of reflectivity (VPR) are derived from the QC'ed reflectivity in native spherical coordinates. A detailed discussion about the computation of VPRs can be found in Zhang et al. (2008). The VPRs are critical in the identification of tropical rain and highly efficient precipitation processes towards producing more accurate QPEs (Xu et al. 2008). Example VPRs for different types of precipitation regimes are shown in Fig.3. The convective VPR (Fig.3a) shows a maximum in reflectivity immediately above the cloud base at ~ 1.5 km (MSL), representing the coalescent growth of large rain droplets (sometimes hail stones) in the convective clouds. Below the cloud base, the reflectivity decreases with decreasing height, representing the breaking of large raindrops and evaporation process. The tropical VPR (Fig.3c), on the other hand, shows gradually increasing reflectivity with the decreasing height all way to the surface, representing a continued growth of a large amount of medium sized raindrops in a very moist environment (Xu et al. 2008). A bright band feature is shown in the stratiform VPR as a peak near the 0°C temperature height (Fig.3b). For cool season stratiform precipitation, radar-derived QPEs often show large overestimation where the lowest radar beams are sampling the bright band and underestimation where the beams are sampling the ice region above the bright band. To mitigate these errors, a real-time VPR correction technique is under development and will be implemented in the NMQ system in winter of 2010.

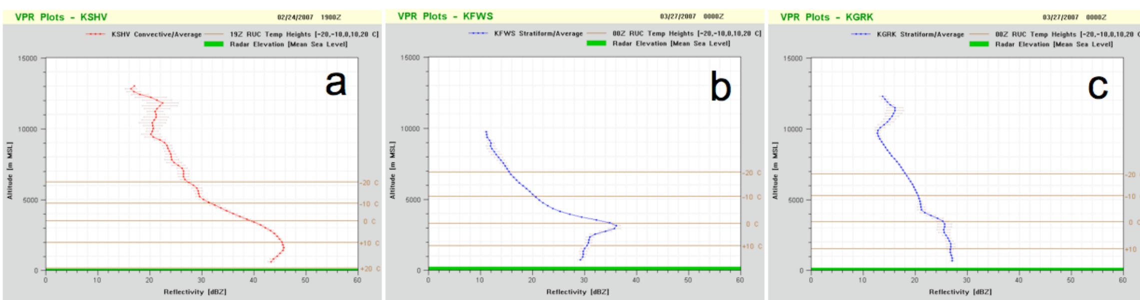

Fig. 3 Example VPRs for convective (a), stratiform (b), and tropical (c) precipitation. The brown lines indicate, from top to bottom, -20, -10, 0, and 10C temperature heights at the radar sites.

From QC'ed single radar reflectivity data, the lowest (altitude) radar bins with valid reflectivity values are found. These constitute a 2-D field that is equivalent to the "hybrid scan" in O'Bannon (1997) and Fulton et al. (1998). The hybrid scan reflectivity (HSR) comes from different heights at different locations because the height of the radar beam increases with range and because beam blockages and terrain clearances vary spatially. Generally, the higher the HSR bin, the less accurate the radar-based precipitation estimates because of non-uniform VPRs.

2.2 Three-dimensional reflectivity mosaic and severe storm products

Single radar reflectivity Cartesian (SRC) grids from multiple radars are combined into a 3-D reflectivity mosaic. An exponential distance weighting function is used when multiple radar observations cover a single grid cell (Zhang et al. 2005). The mosaic grid covers the CONUS and the southern part of Canada (Fig.4), and has the same horizontal and vertical resolutions as the SRC grids. The mosaic domain spans from 130W to 60W in longitude and 20N to 55N in latitude. The grid is in the cylindrical equidistant map projection and has a resolution of 0.01° (longitude) × 0.01° (latitude). The resolution in the x-direction (east-west) is approximately 1.045 km at the southern bound of the domain and approximately 0.638 km at the northern bound of the domain. The resolution in the north-south direction is about 1.112 km everywhere.

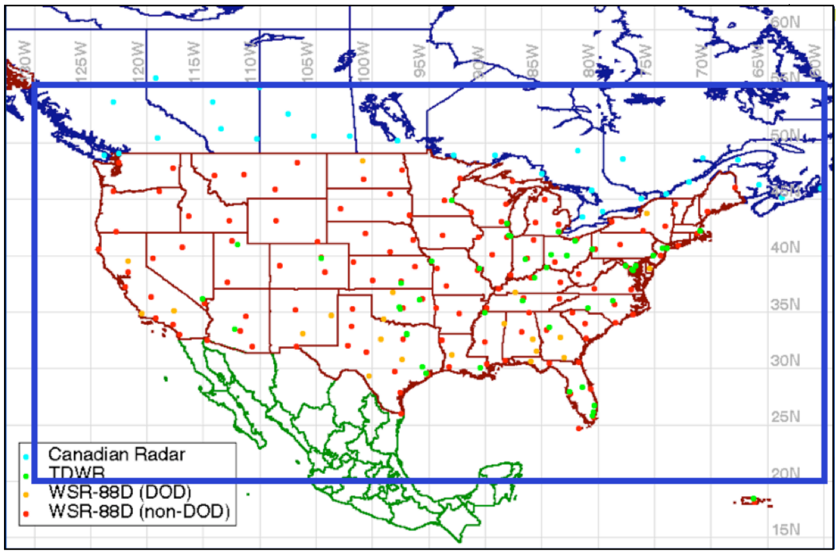

Fig. 4 The NMQ product domain (solid blue box). Dots of different colors represent different radar networks including WSR-88D, Terminal Doppler Weather Radar (TDWR), and Canadian operational radars.

The NMQ system is designed to be adaptive to different radar networks. In the current NMQ system at the NSSL, real-time data from 31 Canadian radars and 1 TDWRs (Terminal Doppler Weather Radar) are ingested and evaluated. The Canadian radar network is being integrated into the 3-D reflectivity mosaic. Future plans including the incorporation of commercial radars, mobile radar observations (e.g., those from NOAA Hydrometeorological Testbed; http://www.etl.noaa.gov/programs/2004/hmt/), and gap-filling radars such as those from CASA (Collaborative Adaptive Sensing of Atmosphere, McLaughlin et al. 2005).

A suite of severe storm products, including probability of severe hail (POSH, Witt et al. 1998), maximum estimated hail size (MEHS, Witt et al. 1998), 18-dBZ echo top, vertically integrated liquid (VIL, Greene and Clarke 1972), and VIL density (VILD, Amburn and Wolf 1997) are calculated form the 3-D reflectivity mosaic grid and the RUC 3-D temperature analysis. Figure 5 shows an example of aforementioned products for a hailstorm that occurred around Wabasha county of Minnesota on 13 Sept. 2007. The 3-D reflectivity grid in conjunction with the environmental 3-D thermal field is also used to identify microphysical processes and to segregate precipitation regimes. A detailed discussion of the classification of precipitation regimes will be given in section *2.3*.

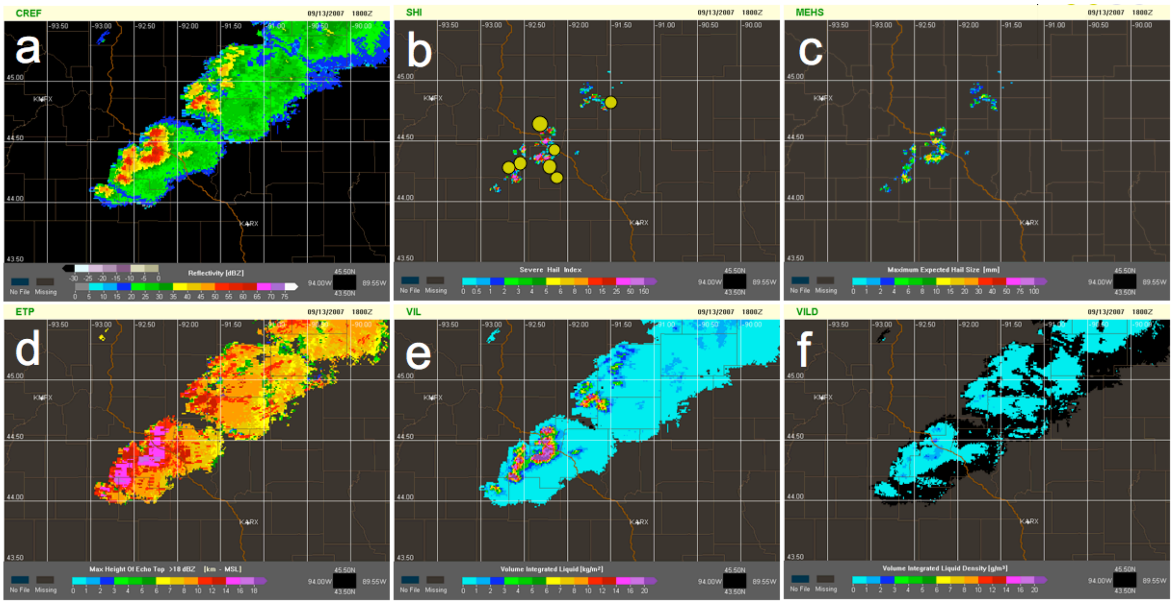

Fig. 5 Example 2-D severe storm products (Composite reflectivity – a; Severe Hail Index – b; Maximum Estimated Hail Size – c; Echo top – d; VIL – e; VIL density – f) from the NMQ system for a hail storm on 13 Sept. 2007 near the Minnesota/Wisconsin boundary. Surface hail verification reports from the NOAA/NWS Storm Prediction Center (*http://www.spc.noaa.gov/climo/reports/yesterday.html*) are overlaid on the top of the Severe Hail Index (SHI) field (b) (yellow circles).

2.3 Q2

2.3.1 Mosaic of hybrid scan reflectivity (HSR)

Single radar hybrid scan reflectivity fields are mosaicked to produce a regional hybrid scan reflectivity field. The HSR mosaic scheme and associated weighting functions are defined below:

$$HSR = \frac{\sum_i w_L{}^i \times w_H{}^i \times SHSR^i}{\sum_i w_L{}^i \times w_H{}^i} \tag{1}$$

$$w_L = \exp\left(-{d^2}/{L^2}\right) \tag{2}$$

$$w_H = \exp\left(-{h^2}/{H^2}\right) \tag{3}$$

Here *HSR* represents the mosaicked hybrid scan reflectivity, *i* is the radar index, *SHSR* is the single radar hybrid scan reflectivity field. There are two components in the weighting function, one for the horizontal (W_L) and another for the vertical (W_H). The variable *d* represents the distance between the analysis point and the radar, and *h* represents the height (above mean sea level) of the single-radar HSR bin. Parameters *L* and *H* are adaptable shape factors of the two weighting functions. This mosaic scheme yields QPE fields with better horizontal continuity than a nearest neighbor approach. The latter can result in discontinuities in mosaicked data fields midway between neighboring radars. The discontinuities are due to factors including different calibration among the radars and different sampling paths from the radars to the overlapping mosaic region.

2.3.2 Classification of precipitation regimes

The classification of precipitation regimes consists of a series of physically based heuristic rules as shown in Fig. 6. Each grid point is assigned a precipitation type based on 3-D reflectivity structure and the environmental thermal and moisture fields. Currently five precipitation types were identified: 1) stratiform rain; 2) convective rain; 3) tropical rain; 4) hail; and 5) snow.

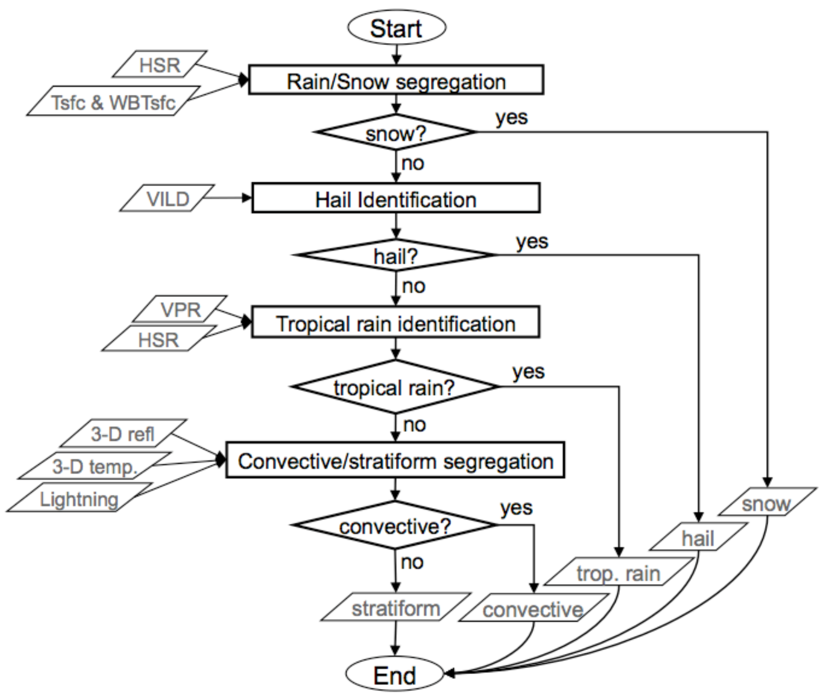

Fig. 6. The precipitation classification process in the NMQ system.

The first step in the precipitation classification is to determine if there is any precipitation at any given grid cell. If the hybrid scan reflectivity at the grid cell is above a threshold (*5 dBZ* if the surface temperature T_{sfc} is below 2°C, and *10 dBZ* otherwise), then it is considered precipitation. If T_{sfc} is below 2°C and the surface wet bulb temperature, WBT_{sfc}, is below 0°C, then the precipitation is considered to be snow. If the precipitation is not snow, then the VIL density (VILD) value is checked for hail. If the VILD value exceeds *1 g/m³* (adaptable), then the precipitation type is labeled as hail.

Tropical rain is identified and delineated using the approach described in Xu et al. (2008). Hourly mean volume scan VPRs from each radar are examined. If the slope of a VPR below the freezing level is negative (i.e., reflectivity increases with decreasing height), then the radar from which the VPR is derived is identified as a "tropical-rain radar". All echoes above an adaptable threshold (default = *35 dBZ*) within an influence radius of the "tropical-rain radar" will be labeled as tropical rain if they are not snow or hail. Further, any echoes above the threshold that are contiguous to the tropical rain region are defined as tropical rain as well. A temperature constraint ($T_{sfc} > 10°C$ [adaptable]) is applied for the tropical rainfall delineation.

A convective and stratiform segregation similar to that in Zhang et al. (2008) is applied to the rest of the precipitation. A pixel is identified as convective if a) reflectivity at any height in the column is greater than *50 dBZ* (adaptable) or b) reflectivity is greater than *30 dBZ* (adaptable) at –10°C height or above. Temperature soundings are obtained from hourly analyses of the RUC model. The remaining echoes that are not identified as snow, hail, tropical rain, or convective rain are classified as stratiform rain.

Figure 7 shows mosaicked HSR and associated precipitation type fields for two events. One event is the Tropical Storm Humberto over Louisiana on 13 Sept. 2007 (Figs. 7a-b);

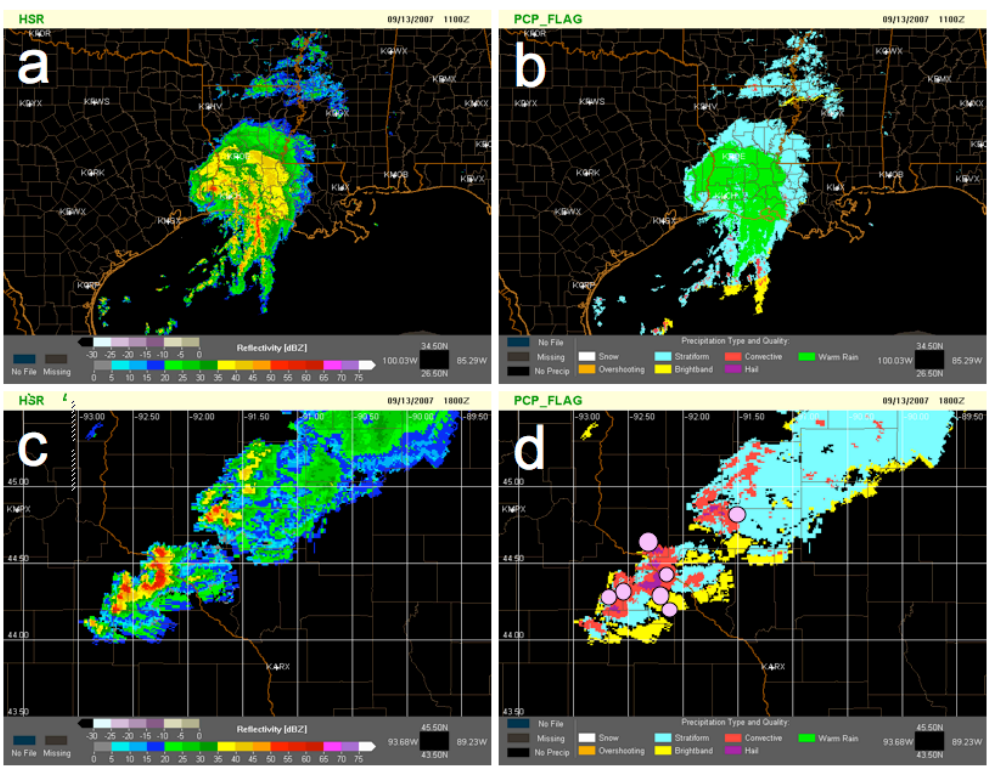

Fig. 7 Mosaic HSR (a, c) and precipitation type (b, d) fields for tropical storm Humberto (a, b) and for a hailstorm event over Wabasha, MN (c, d).

the other is a hailstorm, which passed through Wabasha county of Minnesota in the afternoon of 13 Sept. 2007 (Figs. 7c-d). The NMQ system identified the heavy precipitation bands around the core areas as tropical-rain (Fig.7b). For the Wabasha storm event, hailstones of 3/4 to 1” were reported (pink circles in Fig.7d) between 17:00 to 18:30UTC. The reports correlated well with the hail regions identified by the NMQ system (Fig.7d).

2.3.3 Radar-derived QPEs

Radar-derived precipitation rate is obtained by applying Z-R relationships to the mosaicked HSR field pixel-by-pixel. Four Z-R relationships are used in association with the precipitation type field (e.g., Fig.7):

Convective (Fulton et al. 1998): $Z=300R^{1.4}$ (4)

Stratiform (Marshall et al. 1955): $Z=200R^{1.6}$ (5)

Tropical rain (Rosenfeld et al. 1993): $Z=230R^{1.25}$ (6)

Snow at the surface (Radar Operations Center 1999): $Z=75R^{2.0}$ (7)

Here, Z represent the radar reflectivity in mm^6m^{-3}, and R represents rain rate (Eqs.[4]-[6]) or snow water equivalent (Eq.[7]) in $mm{\cdot}hr^{-1}$. For hail pixels, the convective Z-R is applied with a cap of 49 dBZ (adaptable). A cap (default = 55 dBZ) is also applied to the tropical rain Z-R relationship.

The precipitation rate field is calculated every 5 minutes. Hourly and three hourly accumulations are computed every 5 minutes by aggregating the rate fields. The hourly accumulations are aggregated into 6, 12, 24, 48, and 72 hr QPE every hour on the top of the hour.

2.3.4 Local gauge corrected (LGC) radar-derived QPEs

The local bias correction scheme in the NMQ system is based on the method developed by Ware (2005). The first step in the procedure is to calculate an additive radar rainfall error at each rain gauge location according to the following equation:

$$e_i = r_i - g_i \qquad (8)$$

where e_i is the error at the i^{th} rain gauge, r_i is the radar-estimated rainfall and g_i the gauge observed value at the i^{th} rain gauge. Error values are then interpolated over the pre-defined radar domain using the following equation:

$$R_e = \sum_{i=1}^{n} e_i w_i \Big/ \sum_{i=1}^{n} w_i \qquad (9)$$

where R_e is the estimated radar error at the pixel being interpolated, w_i is the weight assigned to the i^{th} rain gauge, and n represents the total number of matching gauge and radar pixel pairs.

The method used to calculate the weights is a modified version of inverse distance weighting (IDW) found in Simanton and Osborn (1980). The weights are calculated with the following equation:

$$w_i = \begin{cases} 1/d_i^{\,b} & d_i \le D \\ 0; & d_i > D \end{cases} \qquad (10)$$

where d_i is the distance between the radar pixel and the i^{th} rain gauge, b is an exponent, and n is the number of rain gauges within a specified radius, D, of the radar pixel. In a dense rain gauge network, rain gauges that are located far from the radar pixel will have small weights and little effect on the error estimate. However, in regions with sparse gauges, sometimes only one gauge can be used in the interpolation resulting in a constant error within the entire radius of influence. This problem can be alleviated by applying a normal distribution to the error estimates in which the gauge impact is reduced as the distance away from that gauge increases. For each radar pixel the following value is calculated:

$$\alpha = \sum_{i=1}^{n} \exp\left(\frac{-d_i^{\,2}}{(D/2)^2}\right) \qquad (11)$$

where D is the radius of influence, and n is the number of rain gauges within the specified radius (D) of the radar pixel. If the value is greater than 1, then there are a sufficient number of gauges being used to interpolate that point. If the value is less than 1, then the radar estimate is given the remaining weight to equal 1 and the following equation is used for the weighting function:

$$w_i = \begin{cases} \alpha \cdot \dfrac{1}{d_i^{\,b}}; & d_i \le D \\ 0; & d_i > D \end{cases} \qquad (12)$$

where all variables are the same as defined above. This procedure results in more weight being given to the radar estimates in areas of poor rain gauge coverage and at domain boundaries.

Values of the exponent, *b*, and the influence radius, *D*, in the previous equation (12) are obtained by minimizing the mean squared (radar-gauge) error (MSE) using a cross-validation scheme. Initial values of *b* and *D* are selected, and the cross-validation is performed by removing a rain gauge and interpolating to its location using radar-gauge errors at all the remaining rain gauges. The difference between the interpolated radar-gauge error and the observed value is then calculated. After cross-validating all rain gauge points, a total cross-validated MSE is calculated. The two parameters are then adjusted to a new set of trial values and the cross-validation process is repeated. The trial values for *D* can range from ~10 km to 500 km with an adjustment interval of 10 km and *b* can range from 0.5 to 3.0 with an adjustment interval of 0.5. Thus there are a total of $50 \times 6 = 300$ possible combinations of the parameters. The combination that produces minimum cross-validated MSE is considered the best. Cross-validation is performed for each analysis time (i.e., every hour), resulting in different optimum parameters each time.

Anomalously high or low rain gauge values tend to influence adjacent points in the error field because of the nature of interpolation. To remedy this problem, a quality control step is applied to the gauge data. This step removes rain gauges that strongly disagree with the surrounding data so that a spatially consistent precipitation map can be obtained after the local bias correction. For each rain gauge location, all error estimates at radar pixels within a radius of ~10 km are compared with the error value at the gauge. If less than 25% of those error estimates are within a difference threshold, ΔR (default = 5 mm), of the error at the gauge, then the rain gauge is considered problematic. Problematic rain gauges are removed and cross-validation is rerun, which often results in a new set of IDW parameter values. The same procedure is repeated using a smaller difference threshold (e.g., 4 mm) and two more iterations follow, with cross-validation running between iterations. To ensure that a large number of rain gauges are not eliminated, the procedure is terminated if more than 10% of the total number of gauges is omitted.

Fig. 8 shows example 24-hr radar QPEs with and without the local gauge bias correction and the comparison with independent gauge observations. Without the local gauge bias correction, the bias ratio (radar/gauge) of domain mean rainfall is 0.57 (indicating radar underestimation, Fig. 8c) for this event. After the local gauge bias correction, the bias ratio increased to 0.83 (Fig. 8f). The root mean square errors before and after the correction are 0.73 and 0.41, and the correlation coefficients are 0.86 and 0.93, respectively.

In addition to the local-gauge bias corrected radar QPEs, a gauge-only QPE analysis is generated by interpolating gauge observations using the same IDW scheme and same optimal parameters found through the cross-validation process.

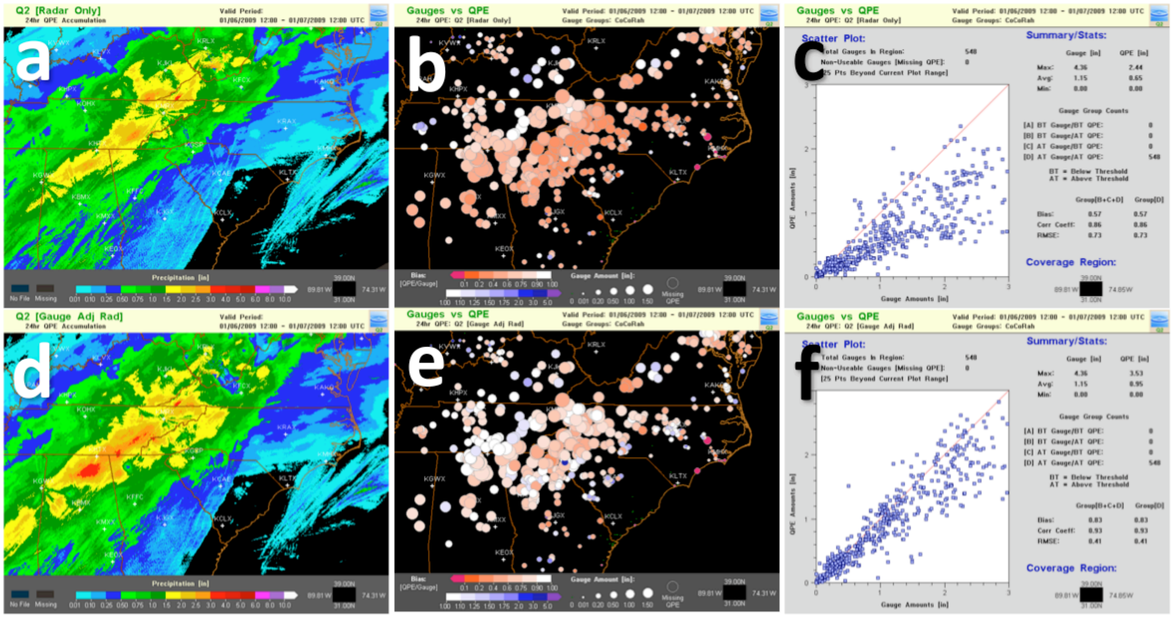

Fig. 8 NMQ 24-hr radar QPEs ending at 12Z on 1/7/2009 in the southeast United States before (a) and after (d) the local gauge bias correction. The bubble charts (b and e) show bias ratios between the QPEs and independent gauge observations, where the size of the circles represents the gauge observed rainfall amount and the color shows the bias. The scatter plots (c and f) shows distributions of the NMQ 24-hr QPEs vs. the gauge observations.

2.4 Evaluations and applications

The current NMQ system contains a real-time evaluation component where the NMQ precipitation products are compared with daily rain gauge observations from the national network of HADS, CoCoRaHS (the Community Collaborative Rain, Hail and Snow Network; http://www.cocorahs.org) as well as several local mesonet rain gauge networks. Various statistics such as bias, correlation coefficient, and root mean square error, are computed between radar-derived QPEs and rain gauge observations. Figure 8 shows examples of evaluation results for an event that occurred on Jan.7, 2009 in the southeast United States. All the NMQ products (Table 1) and the evaluation statistics within one year are kept online and can be viewed from the NMQ website at http://nmq.ou.edu in real-time.

Table 1 List of NMQ products

ID	Unit	Update Cycle	Description
MREF3D	dBZ	5 min	3-D reflectivity field in Cartesian grid
CREF	dBZ	5 min	Composite reflectivity
CREFH	km above MSL	5 min	Height of composite reflectivity
HSR	dBZ	5 min	Hybrid scan reflectivity
HSRH	km above ground	5 min	Height of hybrid scan reflectivity
ETP18	km above MSL	5 min	Echo top of 18 dBZ
SHI	none	5 min	Severe hail index
POSH	%	5 min	Possibility of severe hail
MEHS	mm	5 min	Max estimated hail size
VIL	kg/m^2	5 min	Vertically integrated liquid
VILD	kg/m^3	5 min	VIL density
PCP_FLAG	none	5 min	Precipitation classifications
PCP_RATE	mm/hr	5 min	Precipitation rate
Q2RAD_HSR_1(3)H	mm	5 min	1 (3) -h radar-derived precipitation accumulations
Q2RAD_HSR_6(12, 14, 48, 72)H	mm	1 hr, at the top of the hour	6 (12, 24, 48, 72)-h radar-derived precipitation accumulations
Q2GC_HSR_1(3)H	mm	5 min	1 (3)-h local gauge corrected radar precipitation accumulations
Q2GC_HSR_6(12, 24, 48, 72)H	mm	1 hr, at the top of the hour	6 (12,24, 48, 72)-h local gauge corrected radar precipitation accumulation
Q2GAUGE_1(3,6,12, 14, 48, 72)H	mm	1 hr, at the top of the hour	1 (3, 6, 12,24, 48, 72)-h gauge precipitation accumulation

Users from government agencies, universities and private sectors have applied the experimental NMQ real-time products to various applications. The 3-D reflectivity mosaic component has been implemented at the National Centers for Environmental Prediction for operational data assimilation in the RUC model. It was shown that assimilating 3-D reflectivity data significantly improved the 0-6 hour quantitative precipitation forecasts (Weygandt et al. 2007). The 3-D reflectivity mosaic is also used in aviation icing severity analysis (David Serke, National Center for Atmospheric Research, personal communications). The 2-D composite reflectivity product has been used by Fabry and Seed (2007) for a storm predictability study. The precipitation products are compared to satellite QPEs from the Tropical Rainfall Measurement Mission (Amitai 2009). In 2006, working with the NWS' Office of Climate, Weather, and Water Services, NSSL began prototype testing of the high-resolution gridded Q2 precipitation products as input into the Flash Flood Monitoring and Prediction program (Filiaggi et al. 2002). Dissemination of NMQ QPE products to select River Forecast Centers (RFCs) began in 2007 with all RFCs currently having access through the Advanced Weather Interactive Processing System (AWIPS) Multi-sensor Precipitation Estimator (MPE; Glaudemans et al., 2008). Collaborations are ongoing to assess the utility of NMQ precipitation products in operational hydrological models (Wu and Kitzmiller 2009). In coordination with RFCs, several WFOs are beginning to experiment with NMQ data in their Site Specific Headwater Predictor model (Glaudemans 1997).

3. Future Plans

The future development of the NMQ system include the following:

- Integration of polarimetric radar techniques for identification of non-meteorological targets as well as hydrometeor classifications;
- Systematic quantitative evaluations of the NMQ products in collaboration with the NWS Office of Hydrological Development, Office of Climate, Water, and Weather Services for continued enhancement and advancement of the QPE techniques for use in NWS Forecast Offices and RFC operations;
- Continued research and development on VPR correction for radar-based QPE because non-uniform VPR will remain a challenge even for dual-polarized radar QPEs;
- Continued research and development on merging of multi-sensor QPEs; especially for the mountainous west where radar coverage is limited; and
- Integration of gap-filling radar observations.

4. References

Amburn, S.A. and P.L.Wolf, 1997: VIL Density as a Hail Indicator. *Wea. and Forecasting*, **12**, p473–478.

Amitai, E., 2009: Comparison of TRMM radar rainfall estimates with NOAA Next-Generation QPE. *J. Meteor. Soc. Japan*. **87A**, 109-118.

Benjamin, S.G., D. Devenyi, S.S. Weygandt, K.J. Brundage, J.M. Brown, G.A. Grell, D. Kim, B.E. Schwartz, T.G. Smirnova, T.L. Smith, and G.S. Manikin, 2004: An hourly assimilation/forecast cycle: The RUC. *Mon. Wea. Rev.*, **132**, 495-518.

Fabry, F., and A. Seed, 2007: Quantifying and predicting the accuracy of radar based quantitative precipitation forecasts. *Preprints, The 33rd International Radar Conf.* Amer. Meteor. Soc. 6-10 October 2007, Cairns, Australia. CD-ROM, paper P6B.5.

Filiaggi, M., M. Churma, S. Smith, L. Xin, and M. Glaudemans, 2002: Flash Flood Monitoring And Prediction Version 2.0: Continued AWIPS Modernization. *Preprints 18th Conference on IIPS*, Orlando, Amer. Meteor. Soc., **J7.7**.

Fulton, R., J. Breidenbach, D.-J. Seo, D. Miller, and T. O'Bannon, 1998: The WSR-88D Rainfall Algorithm. *Wea. Forecasting*, **13**, p377–395.

Glaudemans, M., 1997: A local headwater model for operational use in the modernized National Weather Service,. *Preprints13th International Conference, on IIPS*, Long Beach, Amer. Meteor. Soc., **J5.2**.

Glaudemans, M., P. Tilles, and B. Lawrence, 2008: Interactive quality control and operational product generation of hourly multi-sensor precipitation estimates in the NWS. *Preprints 23rd Conference on Hydrology*, New Orleans, Amer. Meteor. Soc., **5B.3**.

Greene, D.R. and R.A. Clark, 1972: Vertically Integrated Liquid Water—A New Analysis Tool. *Mon. Wea. Rev.*, **100**, p548–552.

Lakshmanan, V., T. Smith, , K. Hondl, and G. J. Stumpf, and A. Witt, 2006: A real-time, three-dimensional, rapid updating, heterogeneous technique radar merger technique for reflectivity, velocity, and derived products. *Wea. Forecasting,* **21**, 802–823.

Lakshmanan, V., A. Fritz, T. Smith, K. Hondl, and G. J. Stumpf, 2007: An automated technique to quality control radar reflectivity data. *J. Appl. Meteor.,* **46**, 288–305.

Marshall, J. S., W. Hitschfeld, and K. L. S. Gunn, 1955: Advances in radar weather. *Adv. Geophys*. **2,** 1-56.

McLaughlin, D.J., et al., 2005: Distributed Collaborative Adaptive Sensing (DCAS) for improved detection, understanding and prediction of atmospheric hazards. *Procs of 85th AMS Annual Meeting*, San Diego, California.

O'Bannon, 1997: Using a 'terrain-based' hybrid scan to improve WSR-88D precipitation estimates. *Preprints, The 28th International Conference on Radar Meteorology*, September 7-12, 1997, 506-507.

Radar Operations Center: "GUIDANCE ON SELECTING Z-R RELATIONSHIPS". http://www.roc.noaa.gov/ops/z2r_osf5.asp.

Rosenfeld, D., D.B. Wolff, and D. Atlas, 1993: General Probability-matched Relations between Radar Reflectivity and Rain Rate. *J. Appl. Meteor*: **32**, 50–72.

Simanton, J. R., and H. B. Osborn, 1980: Reciprocal Distance Estimate of Point Rainfall. *J. of the Hydraulics Division, ASCE*, **106**, 1242-1246.

Vasiloff, S., D.J., Seo, K. Howard, J. Zhang, D. H. Kitzmiller, M. G. Mullusky, W. F. Krajewski, E. A. Brandes, R. M. Rabin, D. S. Berkowitz, H. E. Brooks, J. A. McGinley, R. J. Kuligowski, and B. G. Brown., 2007: Q2: Next generation QPE and very short-term QPF. *Bull. Amer. Met. Soc.* **88**, 1899-1911.

Ware, E. C., 2005: Corrections to radar-estimated precipitation using observed rain gauge data. M.S. Thesis, Cornell University, 87pp. [Available from Cornell University Library, 201 Olin Library, Cornell University, Ithaca, NY 14853-5301.]

Weygandt, S., S. Benjamin, and J. Brown, 2007: Radar reflectivity-based initialization of precipitation systems using a diabatic digital filter. *Preprints, The 33rd International Radar Conf.* Amer. Meteor. Soc. 6-10 October 2007, Cairns, Australia. CD-ROM, paper 4A.6.

Witt, A., M.D. Eilts, G.J. Stumpf, J.T. Johnson, E.D. Mitchell, and K.W. Thomas, 1998: An Enhanced Hail Detection Algorithm for the WSR-88D. *Wea. and Forecasting*, **13**, p286–303.

Wu, W., and D. Kitzmiller, 2009: Evaluation of radar precipitation estimates from NMQ and WSR-88D Digital Precipitation Array products: Preliminary results. *Preprints, 34th Conference on Radar Meteorology*, Williamsburg, Amer. Meteor. Soc., P14.4.

Xu, X., K. Howard, and J. Zhang, 2008: An automated radar technique for the identification of warm rain processes. *J. Hydrometeorology*. Accepted.

Zhang, J., S. Wang, and B. Clarke, 2004: WSR-88D reflectivity quality control using horizontal and vertical reflectivity structure. *Preprints, The 11th Conference on Aviation, Range, and Aerospace Meteorology*. Amer. Meteor. Soc. 4-8 October 2004, Hyannis, MA. CD-ROM, paper 5.4.

Zhang, J., K. Howard, and J.J. Gourley, 2005: Constructing three-dimensional multiple radar reflectivity mosaics: examples of convective storms and stratiform rain echoes. *J. Atmos. Ocean. Tech*., **22**, 30-42.

Zhang, J., C. Langston, and K. Howard, 2008: Bright Band Identification Based On Vertical Profiles of Reflectivity from the WSR-88D. *J. Atmos. Ocean. Tech.* **25**, 1859-1872.